Theory and Numerics of Two Synchronized Oscillators

Matt Grau

June 19, 2009

An Undergraduate Senior Thesis
fulfilling the requirements of Ph79.

Abstract

Coupled oscillators are used to model systems such as arrays of lasers or detectors whose response is combined to increase signal strength. I investigated a systems of two coupled oscillators using a model incorporating features such as reactive (non-dissipative) force couplings and amplitude-dependent frequencies. I employed careful numerical simulations to build up intuition about the various behaviors of the model and then studied the model analytically to determine regions of synchronization, a phenomenon in which many oscillators lock their relative phase or frequency to a common equilibrium value. The result of this investigation can be used to motivate the choice of parameter values (such as spread of intrinsic frequencies or coupling strength) of small systems of nanomechanical oscillators currently being designed by Matt Matheny in the Roukes laboratory at Caltech.

Contents

List of Figures

1 Introduction

Numerous physical systems can be modeled by interacting oscillators [6]. An exciting quality of such systems is their ability to oscillate collectively at a common frequency or phase even when the individual oscillators have different intrinsic frequencies or initial phases. This phenomenon is known as *synchronization*. Small groups of oscillators are directly applicable to synchronizing systems, such as lasers that are coupled to increase power output [4], and nanomechanical oscillators, where synchronization to a common frequency can eliminate the inevitable frequency differences arising from imperfections in fabrication [2]. Understanding small numbers of coupled oscillators can be useful in the development of "renormalization group" methods to analyze very large systems (such as the synchronized flashing of fireflies [1]).

The general solution to a system of nonlinear oscillators can be very complicated. However, specific solutions can be obtained by taking the limit as the number of oscillators gets either very large or very small and then simplifying various aspects, such as assuming that only phase matters or assuming some symmetry, such as a coupling between oscillators that is all-to-all [5]. Previous work in this field has focused on the continuum limit of a very large number of oscillators and the limit of very small number of oscillators. In this project I investigate a discrete systems of two nonlinear oscillators.

This paper is organized as follows. After an introduction the devices motivating the body of work presented in this paper, I will derive the terms used in the equations of motion of the model from the physical properties of the device. I then explore the behavior of the equations by finding numerical solutions using explicit iterative methods. The observed behavior is used to develop an intuition then used to approach the model analytically, using methods typical of dynamical equations.

2 Devices

Devices are currently being designed, fabricated and developed by Matt Matheny in Michael Roukes's group at Caltech. There are two different devices currently being worked on.

The first type of device is single beam on a chip made of a thin piezoelectric material sandwiched between a p-doped and n-doped layer of GaAs. The piezoelectric material is off-center, so when a voltage is applied to the piezoelectric layer causing it to expand, it strains the beam and causing it to buckle. The beam is placed on one end of a cavity and probed optically with a laser. As the beam buckles, this changes the cavity length and modulates the power in the cavity, which is then detected by shining the laser on a photodiode. The signal from the photodiode is then amplified and phase-shifted so that is satisfies the Barkhausen criterion for oscillation, and then used to drive the piezoelectric, completing the loop.

The piezoelectric beam is a very clean system. It can be probed optically and achieves a strong signal and a very good signal to noise ratio. The primary disadvantage of this system is that multiplexing is not possible. Multiple oscillating piezoelectric beams on a single chip cannot be

probed by the same laser due to the extreme proximity of chip features compared to the waist of the beam. As the eventual goal of this device is the synchronization of a large number of oscillating beams on a single chip, this optical setup is less useful. The second type of device being developed

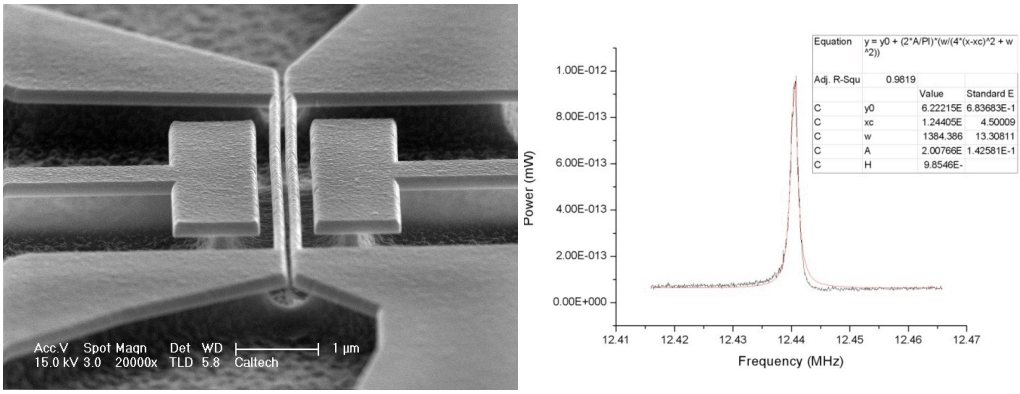

Figure 1: Left: Two beams in the magnetomotive oscillating device. Right: Example closed loop frequency spectrum.

in the Roukes lab is a magnetomotive oscillator, pictured in Fig. 1. In this design a chip containing many fabricated beams is placed in the magnetic field of a strong permanent magnet. AC current is flowed through the beams, causing them to experience a Lorentz force and buckle. The reflected signal of the AC current driving the beams is used to probe the resonators. It is amplified and phase shifted to satisfied the Barkhausen criterion and then fed back into the resonators. While this method does not yield as strong a signal or good signal to noise ratio as the optical design, it can be scaled to drive as many oscillating beams on the same chip as the equipment will allow. The beams may then be coupled by biasing the voltage difference of the beams them to establish an electric field between them. This electric field pulls the beams together, capacitively coupling them.

3 Theory

3.1 Equations of Motion

In this section I will build up the equations of motion used to describe coupled NEM beams. Begin with a harmonic oscillator, which has the equation of motion

$$\ddot{x} + \omega^2 x = 0. \tag{3.1.1}$$

Here $x(t)$ is the displacement (in the case of a beam it is in the flex displacement in the the fundamental mode), and ω is an intrinsic frequency that depends on the the size of the cantilever and it's material properties. For NEMS devices the signal is quite small due to the scale of the devices. In order to increase the signal many devices can be fabricated and coupled together. Because of the

dependence of intrinsic frequency on the size and makeup of each device, intrinsic frequency can vary greatly during actual fabrication of multiple oscillators. It is then important that the devices be *synchronized* so that they oscillate at a single frequency. I will consider the case of two devices reactively coupled. This is done by giving one beam some bias voltage and holding the potential of the other beam to ground. This establishes an electric field between the two beams which pulls them together. Including the coupling term and writing equations for two coupled oscillators, the equations of motion are now

$$\begin{aligned} \ddot{x}_1 + \omega_1^2 x_1 - B(x_1 - x_2) &= 0, \\ \ddot{x}_2 + \omega_2^2 x_2 - B(x_2 - x_1) &= 0, \end{aligned} \tag{3.1.2}$$

where B is proportional to the strength of the coupling force, and ω_1 and ω_2 are the intrinsic frequencies of the separate oscillators. Because the coupling term is proportional to displacement it is invariant under time reversal, and so we call it reactive.

For a spring that obeys Hook's law, stretching or compressing spring with spring constant k and rest length l to new length l' results in a restoring force of magnitude $F = k|l - l'|$. As a toy model for a beam, consider two springs of rest length l, one with endpoints at $(-l,0)$ and $(0,0)$ and the other with endpoints at $(l,0)$ and $(0,0)$. If the springs are connected at $(0,0)$ and then this connected point is displaced to $(0,y)$, then the restoring force will be directed toward $(0,0)$ and have magnitude

$$F = 2kl\left(\sqrt{\frac{y^2}{l^2}+1} - 1\right)\frac{y}{l\sqrt{\frac{y^2}{l^2}+1}} \overset{y \ll l}{\approx} \frac{k}{l}y^3. \tag{3.1.3}$$

This restoring force that has a cubic dependence on displacement which I will refer to as a *Duffing* term. It is a characteristic feature of the Duffing equation, which describes a spring that stiffens as it is stretched,

$$\begin{aligned} \ddot{x}_1 + \omega_1^2 x_1 - B(x_1 - x_2) + a x_1^3 &= 0, \\ \ddot{x}_2 + \omega_2^2 x_2 - B(x_2 - x_1) + a x_2^3 &= 0. \end{aligned} \tag{3.1.4}$$

We will see in the next section that this term causes the intrinsic frequency of the beam to shift as the oscillations grow in amplitude. With the addition of this term the differential equations of motion are nonlinear. Finally, a *Van der Pol* term is added,

$$\begin{aligned} \ddot{x}_1 + \omega_1^2 x_1 - B(x_1 - x_2) + a x_1^3 + \nu(x_1^2 - 1)\dot{x}_1 &= 0, \\ \ddot{x}_2 + \omega_2^2 x_2 - B(x_2 - x_1) + a x_2^3 + \nu(x_2^2 - 1)\dot{x}_2 &= 0. \end{aligned} \tag{3.1.5}$$

This term that drives the system towards a limit cycle with x_n near unity. It is comprised of negative linear damping, which models the energy injected into the system through a feedback loop, and positive nonlinear damping, which models the loses due to friction and other sources.

3.2 Perturbation Theory

Above I assume that a and ν are constant for all oscillators, and that the intrinsic frequency ω_n would be the feature that varied the most across oscillators. This assumption is valid because in the system we are trying to model a and ν are observed to be small, thus any variation is dominated by the variations in ω_n.

In this section we will try to solve (3.1.5) by perturbing away from a harmonic oscillator and then eliminating what are known as "secular" terms. The objective will be to remove the fast, "nearly harmonic" oscillations and focus on the slower nonlinear effects.

If the frequency is expressed as deviations around some center frequency $\omega_n^2 = \omega^2(1+\delta_n)$, then the center frequency ω may be removed by choosing a new timescale $t \to t/\omega$, and scaling the parameters $a \to a\omega^2$, $\nu \to \nu\omega$ and $B \to B\omega^2$. It now is convenient to only write equations for a single fiducial oscillator we are interested in, which I will call $x(t)$, and refer to the oscillator it is coupled to as $\tilde{x}(t)$. I will use the subscripts to refer to a term in a series expansion of $x(t)$. The equation of motion now is written

$$\ddot{x} + (1+\delta)x - B(x-\tilde{x}) + ax^3 + \nu(x^2-1)\dot{x} = 0. \tag{3.2.1}$$

If all the parameters δ, a, ν and B are much smaller than unity we can perturb away from the harmonic oscillator solution with a two timescale approximation. These parameters can be expressed as being small perturbations by scaling them by a small factor $\varepsilon \ll 1$,

$$\ddot{x} + (1+\varepsilon\delta)x - \varepsilon B(x-\tilde{x}) + \varepsilon a x^3 + \varepsilon\nu(x^2-1)\dot{x} = 0. \tag{3.2.2}$$

For $\varepsilon = 0$ this is a simple harmonic oscillator with frequency 1. The proposed solution to this equation is an expansion of $x(t)$ in orders of ε. We will only carry out the calculation to first order in ε. Additionally, we will modulate the harmonic oscillator solution over a much slower time scale with a complex amplitude $A(T)$, where $T = \varepsilon t$, so that $x(t) = A(T)e^{it} + \bar{A}(T)e^{-it}$. The complex conjugate is used to ensure that $x(t)$ is real, as it is a measurable physical quantity. We will treat T as an independent variable from t and express $\dot{A}(\varepsilon t) = \partial A/\partial t = (\partial A/\partial T)(\partial T/\partial t) = \varepsilon \partial A/\partial T = \varepsilon A'(T)$. The derivatives of the proposed solution are,

$$\begin{aligned}
\dot{x}(t) &= iA(T)e^{it} - i\bar{A}(T)e^{-it} + \varepsilon(A'(T)e^{it} + \bar{A}'(T)e^{-it}) + \varepsilon\dot{x}_1(t) + O(\varepsilon^2),\\
\ddot{x}(t) &= -A(T)e^{it} - \bar{A}(T)e^{-it} + 2i\varepsilon(A'(T)e^{it} - \bar{A}'(T)e^{-it}) + \varepsilon\ddot{x}_1(t) + O(\varepsilon^2).
\end{aligned}$$

These are substituted into (3.2.2). We require that all orders of ε must vanish separately. The zeroth order equation is that of the harmonic oscillator and is automatically satisfied by the $e^{\pm it}$ term of $x(t)$. The first order equation is

$$\ddot{x}_1 + x_1 + 2i(A'e^{it} - \bar{A}'e^{-it}) + \delta(Ae^{it} - \bar{A}e^{-it}) - B(Ae^{it} + \bar{A}e^{-it} - \tilde{A}e^{it} + \bar{\tilde{A}}e^{-it}) \\ + a(A^3e^{3it} + 3|A|^2Ae^{it} + 3|A|^2\bar{A}e^{-it}\bar{A}^3e^{-3it}) \\ + i\nu(A^3e^{3it} + (|A|^2 - 1)Ae^{it} - (|A|^2 - 1)\bar{A}e^{-it} - \bar{A}^3e^{-3it}) = 0. \tag{3.2.3}$$

We can identify this equation as the harmonic oscillator equation with periodic forcing terms. The $e^{\pm it}$ term is known as a secular[1] term. This term is a resonant forcing and will cause the amplitude of the corrective term $x_1(t)$ to grow in time. In order for the stated perturbation theory to be faithful to the original assumptions, $x_1(t)$ may not grow to be large, so the secular term must be eliminated. We use the free parameter introduced by the two timescale expansion to set the coefficients of $e^{\pm it}$ to zero: The $e^{\pm 3it}$ does not create a solution that grows in amplitude with time, so there is no need to remove it. Setting the coefficients of the secular term equal to zero, we have

$$2iA' + \delta A - B(A - \tilde{A}) + 3a|A|^2A + i\nu(|A|^2 - 1)A = 0. \tag{3.2.4}$$

This is a first order dynamical equation. We end our perturbation theory here, as this provides the rest of the information of the zeroth order term, and can be used to calculate the first order correction. Define new variables $z(\nu T/2) = A(T)$, $\omega = \delta/\nu$, $\alpha = -3a/\nu$, $\beta = B/\nu$. I will also return to using $\dot{z}$ to mean a time derivative of z, now with respect to the rescaled time $\nu T/2$. The equations for both oscillators written in their entirety are

$$\dot{z}_1 = i(\omega_1 - \alpha|z_1|^2)z_1 + (1 - |z_1|^2)z_1 - i\beta(z_1 - z_2), \\ \dot{z}_2 = i(\omega_2 - \alpha|z_2|^2)z_2 + (1 - |z_2|^2)z_2 - i\beta(z_2 - z_1). \tag{3.2.5}$$

This is a first order system of dynamical equations, which is easy to solve for a given set of $\{z_1(t), z_2(t)\}$ using a Runge-Kutta method to iterate from $\{z_1(0), z_2(0)\}$ with $t/\Delta t$ intermediate steps. Through this perturbation theory we have removed the fast time scale of the harmonic oscillator and left only the slower time scale nonlinear contribution. With the fast time dependence removed we are free to use larger time steps Δt with the Runge-Kutta.

3.3 Numerical Simulation

I performed numerical implicit integration on (3.2.5) using a fourth order Runge Kutta iterative method (RK4) implemented in Python. With this as a base I constructed a library of functions to

[1] I had not previously seen the word "secular" used in this context. I had previously always thought it to refer to something of state or to mean"worldly". It seems that this technical use of the world comes from astronomy, where it is used to mean slow changes in the motion of celestial objects. The etymology of the word is derived from the latin word *saecularis* meaning "of the age". This was extended to long time phenomena, such as celestial mechanics, literally occurring over "ages". In the context I am using it secular refers to the long timescale introduced to allow for the removal of secular terms from the perturbation theory.

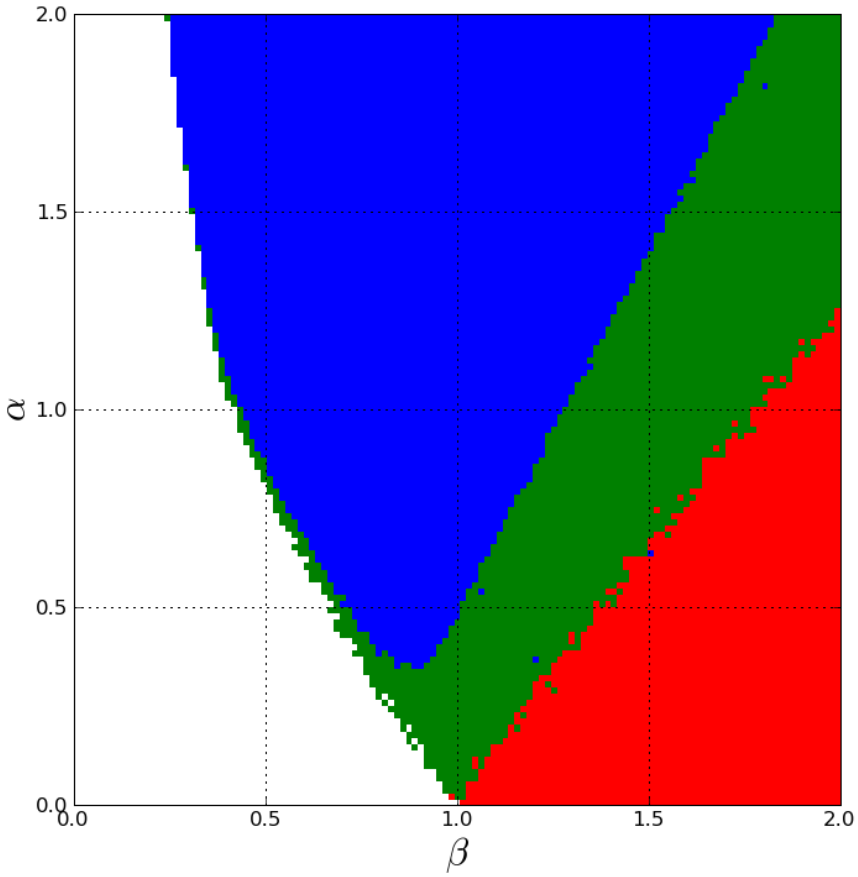

Figure 2: Survey of parameter space.

adiabatically sweep parameters (e.g. Fig. 3) and perform searches of parameter space (e.g. Fig. 2). From performing many numerical calculations we can make several observations that will be essential to describing this system analytically. The first is that there are three classes of behavior:

Phase Locked Synchronization Both oscillators advance in time at a single common frequency. The relative phase between the oscillators is constant.

Unlocked Synchronization The relative phase between the two oscillators is not constant, but phase slips do not occur. The phase of one oscillator never advances more than 2π ahead of the other.

No Synchronization Each oscillator advances in time at it's own frequency, affected by the other oscillator a negligible amount. The relative phase between the oscillators will increase in time without bound.

The second is that for both the locked and unlocked synchronized state there are solutions where the phase difference ϕ of the two oscillators is very close to zero, which I will refer to as "in-phase". There are also solutions where the relative phase ϕ is closer to π, which I will refer to as "anti-phase".

How these three classes occupy parameter space can be seen in Fig. 2. At each (β, α) pair perform RK4 for 15 random initial conditions. The hope here is to explore the space of initial conditions so that at least one of the 15 points is in each of the different basins of attraction for the different classes of behavior. Then the result of the RK is checked to determine what class of behavior occured. If none phase lock, color that point white (no synchronization). If all 15 phase lock with $0 < \phi < \pi/2$ the point is colored blue (a single phase locked state exists here). If all 15 phase lock but for some $\pi/2 < \phi < \pi$ and and $0 < \phi < \pi/2$ for others the point is colored red (two phase locked states exist here). If some, but not all, of the 15 RK phase lock color then that pixel is colored green (both a phase locked and unlocked synchronized state exist here).

This search of parameter space can give us a good idea of what behavior we expect from the oscillators. We first see that exactly what we expect, that they synchronize for large values of the coupling β, and that the nonlinearity α plays some role as well.

The goal in the later sections will be to calculate where the boundary of these regions will occur, and at the same time to understand what causes them. A more detailed view of the boundaries is in Fig. 3. This figure shows very slow sweeps of parameter β, and where transitions occur for a given (β, α) which is plotted as a point on the left plot.

The effect of synchronization on the frequency spectrum of the oscillators is shown in Fig. 4. Here the intrinsic frequency ω_0 of one is held fixed as the other ω_1 is swept from -3 to 5. Between about -1 and 3 the oscillators have phase locked and exhibit a single common frequency. At ω_1 outside this region the spectrum of each oscillator is more diverse as the frequencies of z_1 and z_2 beat.

I also implemented a second order stochastic Runge Kutta (SRK2) in Python for numerical simulations including white noise[3]. I've included a benchmark test of the noise I made to ensure it was a proper stochastic Runge Kutta method, Fig. 5. The sum of the absolute phase of the two oscillators experiences no forces, so in the presence of noise it should undergo a random walk. The expected value of a random walk is proportional to $\sqrt{T}$, so $\langle(\theta_1 + \theta_2)^2\rangle$ should increase linearly in time. I approximate the expected value by averaging 100 SRK runs. This figure shows that for constant time and different number of iterative steps the noise stays constant, proving that this implementation of SRK is correct.

In Fig. 6 an example of the effect of noise on the solutions. This is a sweep of coupling strength like in Fig. 3, but as the amount of noise increases we can see that the jump from the anti-phase unlocked state to the in-phase locked state occurs for stronger couplings.

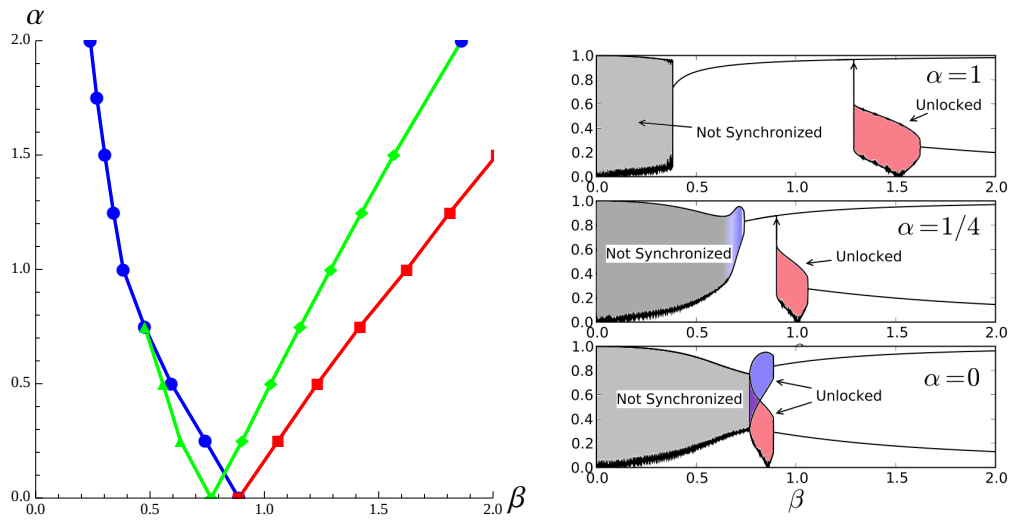

Figure 3: Left: Boundary data obtained from slow sweeps of β for set α and $\Delta\omega = 1$. The blue curve (circles) corresponds to the boundary of the in-phase locked solution. The red curve (squares) corresponds to the boundary of the anti-phase locked solution. The diamonds are the boundary of the anti-phase unlocked solution, and the triangles are the boundary to the in phase locked synchronized state. The sweeps that generated this data are pictured on the right. Right: In these β is slowly swept from 2 to 0 for set α and Δω. Here the excursion of $|z_1 + z_2|/2$ is plotted. When the oscillators are phase locked this should be a single line. When unlocked or not synchronized the excursion will increase, because the amplitudes and phases are changing in time. We can see that there are two phase locked solutions, the in-phase solution where $|z_1 + z_2|/2$ is near 1, and the anti-phase solution, where $|z_1 + z_2|/2$ is near 0. As β is swept from 2 to 0 we see that the anti-phase solution becomes unlocked (shaded red), and then jumps to the in-phase solution. Finally as β is swept lower the in-phase solution unlocks (blue) and synchronization is lost (grey).

```
class stochastic_runge_kutta:
        def __init__(self, data, f, time=0, dt=0.01):
                self.data = array(data)
                        self.time = float(time)
                        self.dt = float(dt)
                        self.f = f
                        self.D = 0

        def step(self,dt,data):
                        """Will take a single SRK2 step of dt from point data"""
                        psi = dot(sqrt(2*self.D*dt),random.normal(size=(2,len(data))))
                         k1 = self.f(self.time,data)
                          k2 = self.f(self.time+dt,data+dt*k1+psi[0]+1j*psi[1])
                          return data + (dt/2)*(k1+k2)+psi[0]+1j*psi[1]
```

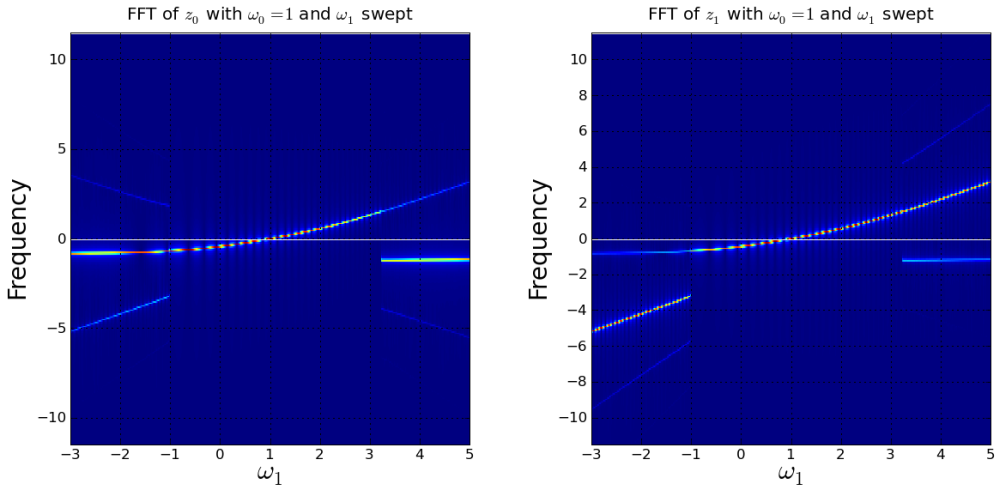

Figure 4: Fourier Transform of oscillators as the intrinsic frequency of one is swept. Red corresponds to higher intensity.

3.4 Analysis

3.4.1 Amplitude Death

Zero amplitude in both oscillators (called *amplitude death*) is a fixed point, but it is unstable. Linearizing (3.2.5) around $|z_1| = |z_2| = 0$ causes all the nonlinear terms to drop out, leaving

$$\begin{pmatrix} \dot{z}_1 \\ \dot{z}_2 \end{pmatrix} = \begin{pmatrix} 1 + i(\omega_1 - \beta) & i\beta \\ i\beta & 1 + i(\omega_2 - \beta) \end{pmatrix} \begin{pmatrix} z_1 \\ z_2 \end{pmatrix}. \tag{3.4.1}$$

By taking the Trace of the Jacobian we find that

$$\lambda_1 + \lambda_2 = Tr \begin{pmatrix} 1 + i(\omega_1 - \beta) & i\beta \\ i\beta & 1 + i(\omega_2 - \beta) \end{pmatrix} = 2 + i(\omega_1 + \omega_2 - 2\beta). \tag{3.4.2}$$

Taking the real part of this equation we see that $Re(\lambda_1 + \lambda_2) = 2$, so at least one eigenvalue will always have a positive real component, causing this fixed point to be unstable. This is a due to the reactive nature of the coupling. If the coupling had a dissipative component then regimes would exist when amplitude death is a stable solution to the model[4]. From this point on I will only consider solutions with non-zero amplitudes.

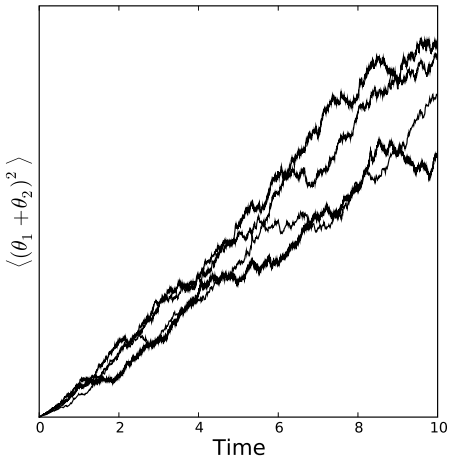

Figure 5: $(\theta_1+\theta_2)^2$ average 100 times with noise and timestep $\Delta t = 0.01, 0.005, 0.0025$,and 0.00125 for constant time.

3.4.2 Amplitude and Phase

If in (3.2.5) $z(t)$ is written as a complex number with amplitude and phase, $z_n(t) = r_n(t)e^{i\theta_n(t)}$, then these equations can be divided through by the complex phase $e^{i\theta_n}$ of each oscillator and then separated into real and imaginary components,

$$\begin{aligned}\dot{r}_1 + i\dot{\theta}_1 r_1 &= i(\omega_1 - \alpha r_1^2)r_1 + (1-r_1^2)r_1 - i\beta(r_1 - r_2 e^{i\phi}),\\ \dot{r}_2 + i\dot{\theta}_2 r_2 &= i(\omega_2 - \alpha r_2^2)r_2 + (1-r_2^2)r_2 - i\beta(r_2 - r_1 e^{-i\phi}).\end{aligned} \tag{3.4.3}$$

We get the amplitude and phase dynamical equations,

$$\dot{r}_1 = (1-r_1^2)r_1 - \beta r_2 \sin\phi, \tag{3.4.4}$$

$$\dot{r}_2 = (1-r_2^2)r_2 + \beta r_1 \sin\phi, \tag{3.4.5}$$

$$\dot{\phi} = \Delta\omega - \left(r_2^2 - r_1^2\right)\left(\alpha + \frac{\beta}{r_1 r_2}\cos\phi\right). \tag{3.4.6}$$

where $\phi = \phi_2 - \phi_1$, and $\Delta\omega = \omega_2 - \omega_1$. We have gone from four equations (two real and two imaginary), to three. This is because dynamical equations for the phase of each oscillator, $\dot{\theta}_1$ and $\dot{\theta}_2$ have been combined into a single dynamical equation for relative phase, $\dot{\phi}$. We are allowed to do this because in this model the dynamics of one oscillator relative to another cannot depend on the overall phase.

These equations have many advantages. The fixed points of (3.4.6) describe a synchronized state that I will refer to as *phase locked*. From numerical simulations it is evident that when the

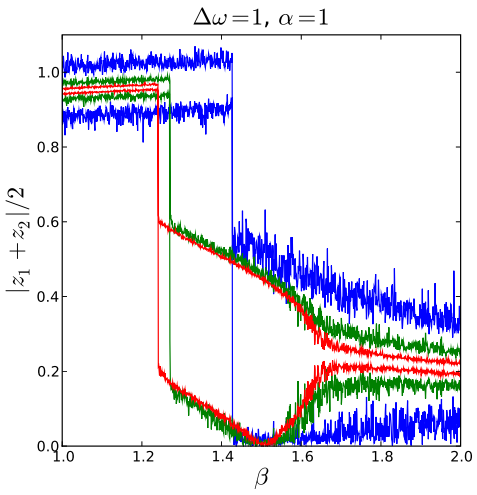

Figure 6: An example of noise affecting the unlocked synchronized state. Blue is noise $D = 10^{-3}$, green is 10^{-4} and red is 10^{-5}. The coupling β is swept from high to low.

oscillators are phase locked it must be true that $\dot{r}_1 = \dot{r}_2 = 0$. I will begin by examining these fixed points.

3.4.3 Symmetries

There are some symmetries in (3.4.4)-(3.4.6). They are useful to simplify the following calculations by reducing the space we must search for stable solutions. The most obvious is that they are invariant under $\phi \to \phi + 2\pi$. There are three other invariant transformations that can be performed on these equations

$$\phi \to -\phi, r_1 \leftrightarrow r_2 \text{ and } \Delta\omega \to -\Delta\omega. \tag{3.4.7}$$

$$\phi \to -\phi, \alpha \to -\alpha, \beta \to -\beta \text{ and } \Delta\omega \to -\Delta\omega. \tag{3.4.8}$$

$$\phi \to \pi + \phi \text{ and } \beta \to -\beta. \tag{3.4.9}$$

3.4.4 Fixed Points

By adding together (3.4.4) and (3.4.5) we find that all other fixed points must lie on the curve (see Fig. 7)

$$r_1^2 - r_1^4 + r_2^2 - r_2^4 = 0. \tag{3.4.10}$$

From this we see that in a phase locked equilibrium state the amplitude of one oscillator must

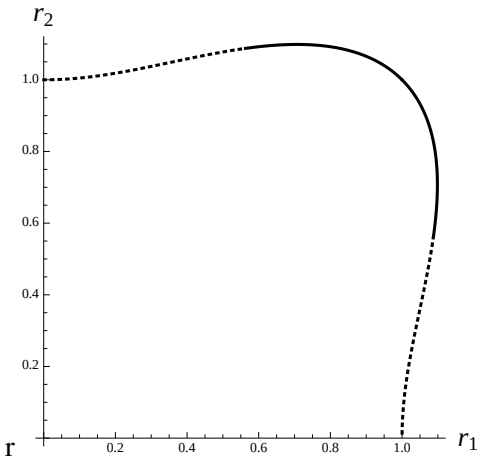

Figure 7: Curve of positive solutions to (3.4.10). The solid curve is $r_1 = s_1, r_2 = s_2$ (3.4.11), and the dotted curve is $r_1 = u_1, r_2 = u_2$ (3.4.12)

be greater than one, and the other less than one. We can break this curve into two parts, by parameterizing r_1 and r_2 with $\xi^2 = 8\beta^2 \sin^2\phi$. The two parts are $\{r_1 = s_1, r_2 = s_2\}$ and $\{r_1 = u_1, r_2 = u_2\}$, where u_1, u_2, s_1, s_2 are functions of parameter ξ and defined as

$$\begin{aligned} s_1 &= \frac{1}{2}\sqrt{3+\sqrt{1-\xi^2} - \mathrm{sign}(\xi)\sqrt{2+\xi^2-2\sqrt{1-\xi^2}}}, \\ s_2 &= \frac{1}{2}\sqrt{3+\sqrt{1-\xi^2} + \mathrm{sign}(\xi)\sqrt{2+\xi^2-2\sqrt{1-\xi^2}}}, \end{aligned} \tag{3.4.11}$$

$$\begin{aligned} u_1 &= \frac{1}{2}\sqrt{3-\sqrt{1-\xi^2} - \mathrm{sign}(\xi)\sqrt{2+\xi^2+2\sqrt{1-\xi^2}}}, \\ u_2 &= \frac{1}{2}\sqrt{3-\sqrt{1-\xi^2} + \mathrm{sign}(\xi)\sqrt{2+\xi^2+2\sqrt{1-\xi^2}}}. \end{aligned} \tag{3.4.12}$$

These are both plotted in (7). The solid curve is s_1 and s_2, and it sweeps from $r_1 = \sqrt{(3+\sqrt{3})/4}, r_2 = \sqrt{(3-\sqrt{3})/4}$ at $\xi = -1$ to $r_1 = \sqrt{(3-\sqrt{3})/4}, r_2 = \sqrt{(3+\sqrt{3})/4}$ at $\xi = 1$, passing through $r_1 = 1, r_2 = 1$ at $\xi = 0$. The dotted curve is u_1 and u_2 and has the same endpoints, although it jumps discontinuously from $r_1 = 1, r_2 = 0$ to $r_1 = 0, r_2 = 1$ at $\xi = 0$.

The fixed point of (3.4.6) is written as,

$$\Delta\omega = \left(r_2^2 - r_1^2\right)\left(\alpha + \frac{\beta}{r_1 r_2}\cos\phi\right) \tag{3.4.13}$$

This is plotted in Fig. 8.

From this plot of fixed points we can immediately see two things. The first is that there are no fixed points for $1 < \xi^2 = 8\beta^2 \sin^2\phi$. For all $\beta > \sqrt{1/8}$ the curves of fixed points split into two, one centered at $\phi = 0$ and the other centered at $\phi = \pi$. This leads us to expect two types of phase locked solutions, one where the two oscillators are "in-phase", and one where the relative phase of the two oscillators is $\phi \sim \pi$, which I shall call "anti-phase". This corresponds to what we see numerically, where the in-phase solution exists in the regions shown in blue, green and red in Fig. 2, and the anti-phase solution exists in the region shown in red.

The second thing we notice is that there are at least two fixed points for any value of $\Delta\omega$. The term $\Delta\omega$ can be thought of as a force pulling the oscillators away from synchronization that has to be balanced by the right hand side of (3.4.13). Because of this we expect for large $\Delta\omega$ that phase locking should not be possible. This suggests checking the stability of these curves of fixed points.

We can use the gap in curves of fixed points to calculate a necessary condition for phase locking. When the discontinuity occurs at $\xi = \pm 1$, (3.4.13) reduces to

$$\pm\Delta\omega = \alpha\sqrt{3\xi/4} \pm \sqrt{2\beta^2 - \xi/4}. \tag{3.4.14}$$

Alternatively written as a curve that we can plot against the numerical data, $\alpha(\beta)$,

$$\alpha = \frac{\sqrt{8\beta^2 - 1} - 2\Delta\omega}{\sqrt{3}}. \tag{3.4.15}$$

This is an necessary condition for phase locking, but not sufficient. It is plotted as a green curve in Fig. 13. We can see that it does not do a very good job of describing where phase locking ends, but we should notice that it always lies to the left (weaker coupling) of phase locking. The linear stability of the fixed points along this line have to be considered in order to determine if a phase locked fixed point will be a solution in a physical system.

3.5 Linear Stability

Linearizing (3.4.4)-(3.4.6) around the fixed points yields

$$\begin{bmatrix} \dot{r}_1 \\ \dot{r}_2 \\ \dot{\phi} \end{bmatrix} = \begin{pmatrix} 1 - 3r_1^2 & -\beta\sin\phi & -r_2\beta\cos\phi \\ \beta\sin\phi & 1 - 3r_2^2 & r_1\beta\cos\phi \\ 2\alpha r_1 + \frac{\beta}{r_1^2 r_2}\left(r_1^2 + r_2^2\right)\cos\phi & -2\alpha r_2 - \frac{\beta}{r_1 r_2^2}\left(r_1^2 + r_2^2\right)\cos\phi & \frac{\beta}{r_1 r_2}\left(r_2^2 - r_1^2\right)\sin\phi \end{pmatrix} \begin{bmatrix} r_1 \\ r_2 \\ \phi \end{bmatrix}. \tag{3.5.1}$$

The three eigenvalues of the Jacobian in (3.5.1) can be evaluated along the solution curves (3.4.11) and (3.4.12) to yield eigenvalues that are functions of the three parameters, α, β and $\Delta\omega$, and ϕ. When the real part of these functions are all negative for a given point in parameter space and value of ϕ then that solution is stable for that value of ϕ. As soon as any of these functions has

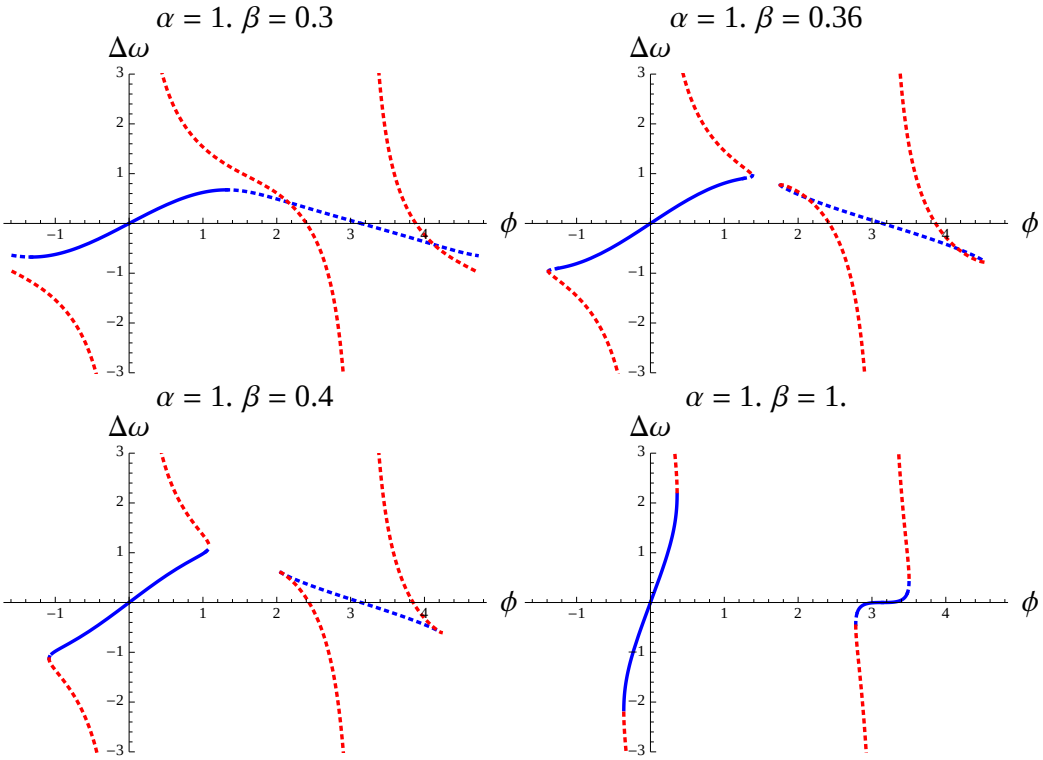

Figure 8: Plots of $\Delta\omega$ as a function of ϕ for a constant value of $\alpha = 1$ and β values of 0.3, 0.36, 0.4 and 1. Every point along these curves are fixed points for a given set of parameters $\Delta\omega, \alpha, \beta$. The red curves correspond to (3.4.13) evaluated with $r_1 = u_1$ and $r_2 = u_2$ (3.4.12), and the blue line corresponds to evaluations with $r_1 = s_1$ and $r_2 = s_2$ (3.4.11). The dotted portions of the curves represents fixed points which are unstable. The stability was calculated by evaluating the Jacobian (3.5.1) for each point ϕ along the curve $r_1 = s_1, r_2 = s_2$ or $r_1 = u_1, r_2 = u_2$. We see that the set of fixed points where $r_1 = u_1, r_2 = u_2$ is always unstable. We also see that the in-phase locked solution is stable for small enough $\Delta\omega$, and that the anti-phase solution has a minimum β for which it is stable.

a real part greater than zero the solution is unstable.

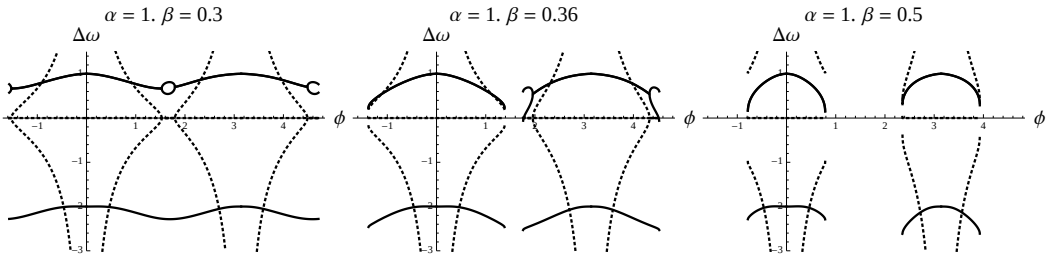

Figure 9: Eigenvalues of (3.5.1) as a function of ϕ, evaluated at $r_1 = u_1$ and $r_2 = u_2$. Notice that at least one of the eigenvalues always has a positive real component for all values of ϕ. The solid curves are the real components of the eigenvalues, and the dotted curves are the imaginary components.

In Fig. 8 this calculation is used to show the stability of the fixed points. Stable fixed points are a solid curve, and the unstable fixed points are a dotted curve. We can see that the set of fixed points where $r_1 = u_1$ and $r_2 = u_2$ (3.4.12) are always unstable. This can also be seen from plotting the eigenvalues, as in Fig. 9, where there is an eigenvalue with a positive real component for all values of ϕ. The set of fixed points where $r_1 = s_1$ and $r_2 = s_2$ is sometimes stable. The eigenvalues are plotted in Fig. 10.

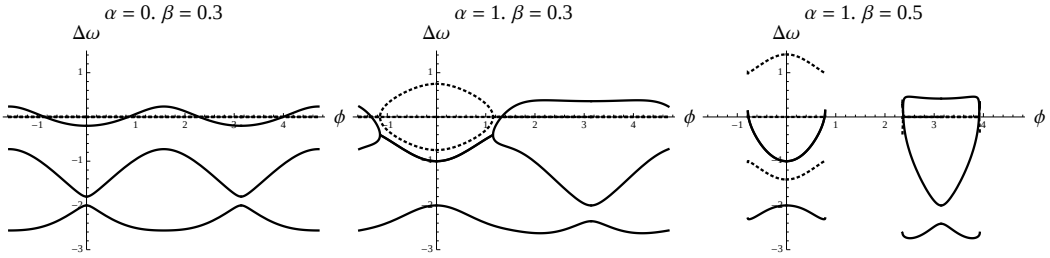

Figure 10: Eigenvalues of (3.5.1) as a function of ϕ, evaluated at $r_1 = s_1$ and $r_2 = s_2$. The solid curves are the real components of the eigenvalues, and the dotted curves are the imaginary components.

We will proceed by using the stability of the $r_1 = s_1, r_2 = s_2$ branch of fixed points to try to define the region in parameter space where phase locking will occur. For a given α and β, invert (3.4.13) to find $\phi(\alpha, \beta, \Delta\omega)$. This has to be done numerically. It is actually rather tricky[2], as there are many roots for each solution curve. Using ϕ, r_1 and r_2 can be evaluated, which can then be

[2]For an example, consider Fig. 8, $\beta = 0.3$. For $\Delta\omega = 0.5$ there are two solutions on the interval $\phi \in [0, \pi/2], r_1 = s_1, r_2 = s_2$. They are $\phi \approx 0.72$ (which results in a stable solution) and $\phi \approx 1.98$ (which is unstable). It is quite a problem to make sure that the root finding method used to invert $\Delta\omega(\phi)$ gives the ϕ resulting in the stable solution. Currently I know no perfect way to do this, other than possibly writing a specialized root finding routine for this specific curve.

used to evaluate the Jacobian. The eigenvalues can be found numerically and then used to make a contour along which the largest eigenvalue is equal to zero. This should be a curve in parameter space defining the boundary of the phase locked region.

The Mathematica code used to create the plots is

```
ContourPlot[0 == Max[Re[Eigenvalues[J[α, β, ϕ] /. FindRoot[Δω − (r2^2 − r1^2) (α + β/(r1 r2) Cos[ϕ])]
/. r1 → s1[ξ] /. r2 → s2[ξ] /. ξ → √8 β Sin[ϕ]]],{α,0,2},{β,0,2}]
```

We expect two type of solutions, in-phase and anti-phase, characterized by two separate cases, where $-\pi/2 < \phi < \pi/2$ and $\pi/2 < \phi < 3\pi/2$. Because we are root-finding along the curves in Fig. 8, a task for which we will require continuity, we will consider the two cases separately.

1. In-Phase Locked: $-\pi/2 < \phi < \pi/2$

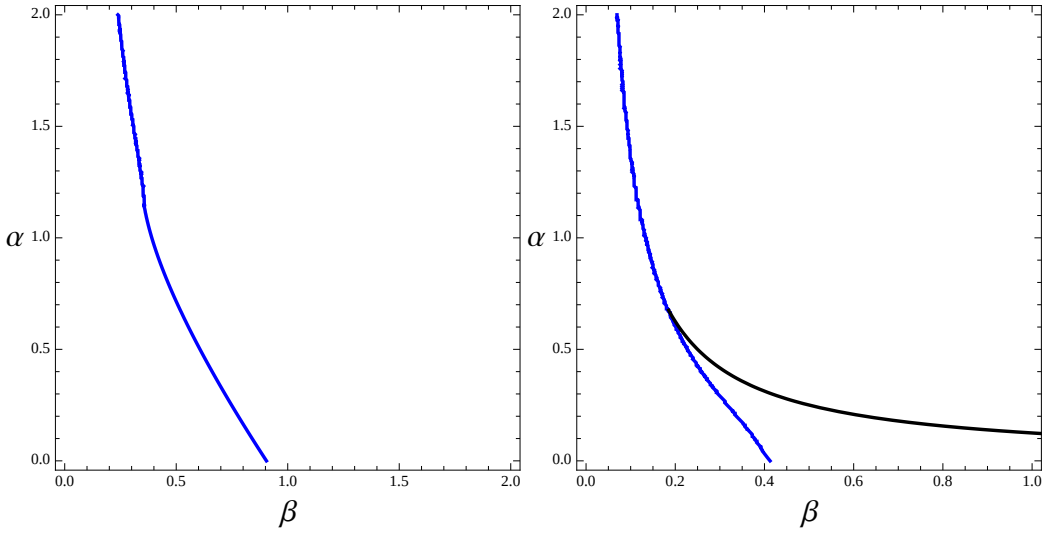

Figure 11: Shown on the left: curve of critical stability for the in-phase locked state with $\Delta\omega = 1$. Shown on the right: curve of critical stability for the in-phase locked state with $\Delta\omega = 1/4$ compared to the $\beta \ll 1$ approximation (3.5.4).

From Fig. 8, we can see that $\Delta\omega$ is always negative when $\phi < 0$. We need only consider $\Delta\omega > 0$, because (3.4.7) is just a relabeling of r_1 and r_2. We need only consider $\phi \in [0, \sin^{-1}(2\sqrt{2}\beta)^{-1}]$ for inverting $\Delta\omega$.

We now try to obtain a contour in parameter space where the largest eigenvalue is zero. This will be the edge of the regions where the phase locked solution is stable and unstable. This is done by plotting contours of the determinant of the Jacobian (3.5.1) in the (β, α) plane, evaluated at for constant $\Delta\omega$ and at each point in the plane. The Jacobian depends on r_1, r_2 and ϕ. Along this chosen curve we have parameterized r_1 and r_2 as a function of ϕ, β and α. We need only ϕ, which is a function of $\Delta\omega$. This function is found numerically by finding the roots of (3.4.13). The result of this procedure is shown is Fig. 11.

If we linearize the curve (3.4.10) near $\xi = 0$, we can approximate r_1 and r_2 as $r_1 = 1+\delta$ and $r_2 = 1-\delta$, where $\delta \ll 1$. This is motivated by Fig. 7, where the slope of the curve around $r_1 = 1, r_2 = 1$ is -1. Plugging these into (3.4.4) and (3.4.5) and only keeping terms out to first order in δ we get

$$2\delta + \beta \sin\phi = \pm\delta\beta\sin\phi. \tag{3.5.2}$$

If we assume that $\beta \ll 1$ then we find that $\delta = -\frac{1}{2}\beta\sin\phi$. Plugging this into (3.4.6) and keeping terms out to first order in δ we find

$$\Delta\omega = -4(\alpha+\beta\cos\phi)\delta = 2(\alpha+\beta\cos\phi)\beta\sin\phi. \tag{3.5.3}$$

The response to $\Delta\omega$ is maximized at $\phi = \pi/2$. For $\Delta\omega$ beyond that there is no ϕ large enough to balance the frequency difference and allow for synchronization. Thus the boundary between phase locking and unlocked should occur at $\phi = 2\pi$. This gives a guess that is good for $\beta \ll 1$,

$$\Delta\omega = 2\alpha\beta. \tag{3.5.4}$$

Plotting this next to the phase locking boundary calculated from the linear stability of fixed points should yield good agreement for small β (less than about 0.2), see in Fig. 11.

2. Anti-Phase Locked: $\pi/2 < \phi < 3\pi/2$

   As in the previous case, $\Delta\omega$ is only positive in one region for ϕ, when $\phi > \pi/2$. Thus we need only consider $\phi \in [\pi - \sin^{-1}(2\sqrt{2}\beta)^{-1}, \pi]$ and $\phi \in [\pi, \pi + \sin^{-1}(2\sqrt{2}\beta)^{-1}]$. The results of the rootfinding are shown in Fig. 12.

3.6 Putting it all together

To characterize this system, we need to combine Fig. 11,12 into one picture that will tell us for what regions of parameter space different phase locked solutions will be stable or unstable. By plotting these curves we construct a picture of the stability of all the solutions , shown in Fig. 13. In this figure we can see the two types phase locked states that exist, plotted in blue for $0 < \phi < \pi/2$ and red for $\pi/2 < \phi < \pi$. The agreement with the data from Runge-Kutta is very good.

Additionally we can see that curve defining the boundary for existence of phase-locking [(3.4.15) shown in green] has good agreement with the points where the unlocked, but still synchronized, solution ceases to exist. Why this occurs is explained in the next section.

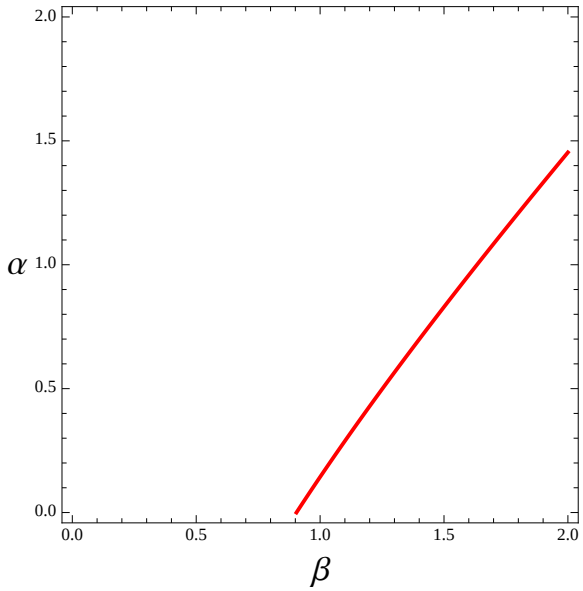

Figure 12: Curve of critical stability for anti-phase locked state with $\Delta\omega = 1$.

3.7 Unlocked Synchronization

The fact that the unlocked synchronized states lie on the edge of the phase locked states in parameters space is a big hint as to their origin. Phase locking can no longer occur when the phase locked fixed point becomes unstable. However, the phase locked solution still exists. I propose that when the the solution becomes unstable, nearby there is a stable limit cycle around the fixed point. The existence of such a limit cycle could be checked by extending the stability analysis to quadratic order. Alternatively, we can first check numerically. We do indeed see that the unlocked synchronized states are stable limit cycles around the now unstable phase locked fixed points. An example is shown in Fig. 14. This is for $\beta = 1.62$, and the fixed point becomes unstable at roughly $\beta = 1.63$. At $\beta = 1.62$ the eigenvalue in the r_1 and r_2 direction have of a positive real component, and they are is $\lambda_{\pm} = 0.0113 \pm 2.908i$. We expect the oscillation frequency of the limit cycle to be the imaginary part of the eigenvalue, $\omega_{lc} = 2.908$, and this is what we see. The discrete Fourier transform is that of the synchronized frequency of both oscillators ($\theta_1 = \theta_2 = 4.743$), beating against the frequency of the limit cycle, yielding peaks in the Fourier transform at increments of 2.908 away from the central peak. By looking at the time evolution of r_1, r_2 and ϕ we see that they are essentially sinusoids with the limit cycle frequency. We expect r_1 and r_2 to oscillate at ω_{lc}, as those are the directions with the imaginary component of the eigenvalue. The reason ϕ also oscillates at this frequency is that to stay a solution ϕ must adjust itself to follow r_1 and r_2. Since there is only one frequency present ϕ must adjust itself at that frequency.

This same reasoning also explains the in-phase unlocked state. However, in this case, (3.4.15) stops at $\beta = 1/\sqrt{8}$. For $\beta < 1\sqrt{8}$ there is always a solution to (3.4.13) for a given value of ϕ (and

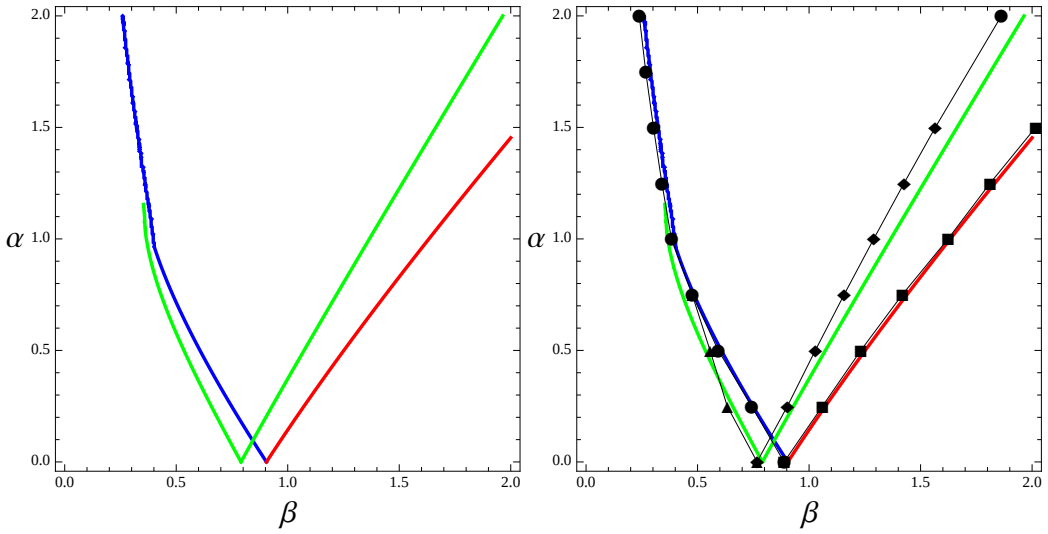

Figure 13: Curves of critical stability for $\Delta\omega = 1$ composed from Fig. 11 and 12. Additionally, the necessary condition for phase locking (3.4.15) is plotted in green. On the right these curves are compared to the data from numerical solutions in Fig. 3.

as long as $\Delta\omega$ is not too large). From Fig. 10 we can see that the imaginary part of the eigenvalues is zero when $\beta < 1/\sqrt{8}$, so there is no oscillating solution.

The limit cycle around the unstable fixed point can be thought of as a perturbation away from the fixed point, with $r_1(t) = r_1^{(0)} + \varepsilon r_1^{(1)} e^{i\omega_{lc}t} + \varepsilon \bar{r}_1^{(1)} e^{-i\omega_{lc}t} + \varepsilon^2 r_1^{(2)}(t) \ldots$ (and likewise for r_2 and ϕ). Naturally a first order perturbation, assuming that r_1, r_2 and ϕ all oscillate around $r_1^{(0)}, r_2^{(0)}$ and $\phi^{(0)}$ with a common, constant frequency will only be valid very close to the boundary where the phase locked solution becomes unstable. As long as the perturbation is valid, then the limit cycle should disappear when the fixed point disappears, because there is no longer anything to perturb away from. Thus the curve (3.4.15) should be a good estimate of when the unlocked synchronized state should disappear, as long as it is close enough to (11) (or (12), depending on which unlocked state we are trying to find the boundary for). Further away from the phase locked boundary the limit cycle becomes more complicated. The annihilation of the phase locked fixed point is a global phenomenon and may no longer correlate with the annihilation of the limit cycle if it is sufficiently pulled away from the perturbation. This argument explains the agreement present in Fig. 13.

This argument could be made more rigorous. A stability analysis out to second order could confirm the existence of limit cycles as solutions. To check the stability of the limit cycles the calculation must be done to cubic order.

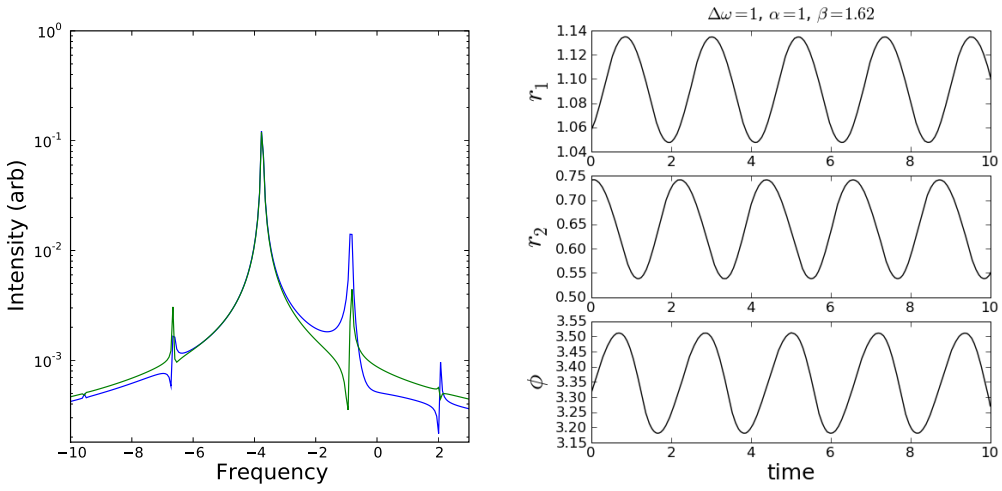

Figure 14: Left: Fourier transform of z_1 and z_2 at $\Delta\omega = 1, \alpha = 1, \beta = 1.62$, when the oscillators are in the unlocked synchronized state. Right: r_1, r_2 and ϕ.

4 Conclusions

In this thesis we have successfully characterized the behavior of our model. We fully explored the observed behavior and classified the solutions into two synchronized states, an the in-phase and anti-phase solutions. These solutions exist as phase locked synchronized states for large coupling strengths, and as unlocked synchronized states for smaller couplings before coming completely unlocked. I've also developed the numerical tools necessary to run simulations of the oscillators with noise.

The very first thing to be done in followup is to wait with anticipation for the multiplexed device to be built and then compare how well its physical behavior matches what we expect based on our calculations. Once this is finished there will surely be a lot of work still to be done on the two oscillator device and model.

The long term goal for these devices seems to be building as many beams on a chip as possible and then synchronizing or driving them in exotic ways to do useful things. The next logical step would be to extend this work to describe a one dimensional array of oscillators coupled to their nearest neighbors. The two oscillator result can be incorporated into a Renormalisation Group technique and then applied to a large nearest neighbor coupled array.

5 Acknowledgements

First, my mentor and advisor, Mike Cross. He is entitled to 10% of the profits. Thanks to Matt Matheny for building the actually oscillators this theory applies to and for providing all of the wonderful device pictures (1). He also took the time to show me his devices and explain everything about them to me, and for that I am indebted to him.

This project will hopefully end with this thesis, but it began as a Caltech SURF project. In addition to Mike Cross I was mentored by Mason Porter, who always demanded near perfection but less often received it from me. Additionally, Jeff Rogers and Ron Lifshitz were great to talk to about my project. I also want to thank the Caltech SURF Office and Program, as well as Boeing for funding. I hope that someday they get their theory of the airplane.

References

[1] J. Buck and E. Buck. *Synchronous fireflies*. Scientific American, 1974.

[2] Michael C. Cross, Jeffrey L. Rogers, Ron Lifshitz, and Alex Zumdieck. Synchronization by reactive coupling and nonlinear frequency pulling. *Physical Review E*, 73(036205), 2006.

[3] Rebecca L. Honeycutt. Stochastic runge-kutta algorithms. i. white noise. *Phys. Rev. A*, 45, 1992.

[4] Jeffrey L. Rogers. Analysis of three coupled limit-cycle oscillators. Preprint, January 2007.

[5] Steven Strogatz. From Kuramoto to Crawford: Exploring the onset of synchronization in populations of coupled oscillators. *Physica D*, 143:1–20, 2000.

[6] Steven Strogatz. *Sync: The Emerging Science of Spontaneous Order*. Hyperion, 2003.